frontiers in Nanotechnology

ORIGINAL RESEARCH
published: 26 November 2020
doi: 10.3389/fnano.2020.584233

Proof of Concept Study: Mesoporous Silica Nanoparticles, From Synthesis to Active Specific Immunotherapy

Stephanie Seré[1], Ulrique Vounckx[2], Jin Won Seo[3], Ilse Lenaerts[4], Stefaan Van Gool[5] and Jean-Pierre Locquet[1]**

[1] Functional Nanosystems, Department of Physics and Astronomy, Katholieke Universiteit Leuven, Leuven, Belgium, [2] Design and Synthesis of Inorganic Materials, Department of Chemistry, Hasselt University, Hasselt, Belgium, [3] Functional Nanosystems, Department of Materials Engineering, Katholieke Universiteit Leuven, Leuven, Belgium, [4] TRANSfarm, Science Engineering and Technology Group, Katholieke Universiteit Leuven, Leuven, Belgium, [5] Translational Oncology, Immunologisch Onkologisches Zentrum Köln, Köln, Germany

OPEN ACCESS

Edited by:
Jianhua Zhang, Tianjin University, China

Reviewed by:
Timothy John Mahony, The University of Queensland, Australia
Ajeet Kaushik, Florida Polytechnic University, United States

***Correspondence:**
Stephanie Seré
stephanie.sere@kuleuven.be
Jean-Pierre Locquet
jeanpierre.locquet@kuleuven.be

Specialty section:
This article was submitted to Biomedical Nanotechnology, a section of the journal Frontiers in Nanotechnology

Received: *16 July 2020*
Accepted: *21 October 2020*
Published: *26 November 2020*

Citation:
Seré S, Vounckx U, Seo JW, Lenaerts I, Van Gool S and Locquet J-P (2020) Proof of Concept Study: Mesoporous Silica Nanoparticles, From Synthesis to Active Specific Immunotherapy. Front. Nanotechnol. 2:584233. doi: 10.3389/fnano.2020.584233

Nanomaterials are increasingly valued tools in drug delivery research as they offer enhanced stability, controlled release and more effective drug encapsulation. Though yet to be introduced in clinical trial, mesoporous silica nanoparticles are promising delivery systems, due to their high chemical and mechanical stability while remaining biodegradable. This work provides proof of concept for particle based vaccines as cost-effective alternatives for dendritic cell immunotherapy. Synthesis and surface chemistry of the nanoparticles are optimized for protein conjugation and nanoparticles are characterized for their physicochemical properties and biodegradation. Ovalbumin is used as a model protein to load nanoparticles to produce a nanovaccine. The vaccine is tested *in vitro* on dendritic cultures to verify particle and vaccine uptake, toxicity, maturation effects and explicitly ovalbumin cross-presentation on MHC class I molecules. The optimized synthesis protocol renders reproducible mesoporous silica nanoparticles, resistant against agglomeration, within the required size range and have carboxylic surface functionalization necessary for protein conjugation. They are biodegradable over a time span of 1 week. This period is adjustable by changing synthesis parameters. UV sterilization of the particles does not induce quality loss, nor does it have toxic effects on cells. Treatment with mesoporous silica nanoparticles increases expression of MHC and costimulatory molecules of dendritic cells, indicating an adjuvant effect of nanoparticles on the adaptive immune system. Nanovaccine uptake and cross-presentation of ovalbumin are observed and the latter is increased when delivered by nanoparticles as compared to control conditions. This confirms the large potential of mesoporous silica nanoparticle based vaccines to replace dendritic-based active specific immunotherapy, offering a more standardized production process and higher efficacy.

Keywords: nanoparticles, characterization, biodegradation, immunotherapy, dendritic cells, cross-presentation

1. INTRODUCTION

Cancer is a leading cause of morbidity and mortality with ∼18 million new cases and 9.6 million cancer-related deaths worldwide in 2018. The number of new cases is expected to rise globally by 70% over the next decade according to the world health organization. Immunogenic tumors, such as breast and prostate cancer are among the leading cancer types in terms of the number of new cases, with 2.1 and 1.3 million diagnoses in 2018, respectively (IARC, 2018). Additionally, cancer is known to be a costly illness to the patient and the overall health care system.

Over the past decades, the role of the immune system in the development and maintenance of tumors was unraveled (Van Gool, 2015). On this basis, cancer immunotherapy emerged as an innovative treatment for immunogenic tumors. It intents to activate or stimulate components of the immune system against the tumor, while minimizing off-target effects as compared to agents that directly kill cancer cells, such as chemotherapy. A plethora of immunotherapeutic approaches is available, but the general goal of immunotherapy is to destroy remaining cancer cells and prevent tumor regrowth (Van Gool, 2015; Riley et al., 2019). One particularly promising approach is active specific immunotherapy based on autologous dendritic cells (DCs) loaded with autologous tumor lysate. DC vaccination is nowadays combined with standard treatment in Phase II and Phase III clinical trials for the treatment of immunogenic tumors, such as prostate cancer, ovarian cancer, glioblastoma, among others. It was demonstrated that these vaccines are safe, elicit an anti-tumor immune response and control tumor growth (Van Gool and De Vleeschouwer, 2012; Dejaegher et al., 2014; Galluzzi et al., 2014; Makkouk and Weiner, 2015). Unfortunately, these responses did not significantly improve subsequent clinical outcomes. Reintroducing DCs from the *ex vivo* cell culture into the immunosuppressive environment of the patient probably affects their viability and functionality (Le Gall et al., 2018). Therefore, an effort should be made to increase the efficacy of the vaccine to obtain higher long term survival rates. Moreover, the small-scale production process of DC-based vaccines is expensive, with an estimated cost of 20,500 euros per patient (Van de Velde et al., 2014; Le Gall et al., 2018). One solution is the development of an off-the-shelf, universal drug delivery system (DDS) that carries tumor lysate and immunomodulatory agents to target DCs *in vivo*.

The development of DDSs is a research field of all times. The need for more efficient encapsulation and controlled-release technologies increased, due to the development of new drugs often with poorer stability in biological environments, higher dose sensitivities and larger molecular sizes (Barbé et al., 2004). In the drug delivery research field, nanoparticles (NPs) have been a hot topic for almost 20 years due to their quantum mechanical properties, high surface to volume ratio and therefore relatively large functional surface to bind and carry drugs or probes (De Jong and Brom, 2008). NPs come in all shapes and sizes, but not all of them are suitable for (bio)medical applications. Specifically considering drug delivery, biocompatibility or biodegradability of the NPs is required to release their cargo at the targeted site and reduce or eliminate potential risks. The majority of research on NP-based DDSs focuses therefore mostly on liposomes, micelles and polymeric particles. The NP-based DDS can be specifically chosen and optimized depending on the drug, route of administration and desired pharmacokinetics. Liposomes consist of a lipid bilayer, which is also an important component of the cell membrane. Therefore, research on this type of particles began and developed very early (Delves, 1998). Micelles offer a relatively simple synthesis procedure, as they are formed through self assembly of amphiphilic molecules at a critical micelle concentration (Marasini et al., 2017; Mitra et al., 2017). Liposomes and micelles gained large interest as DDS because they enable encapsulation and delivery of hydrophilic and hydrophobic agents, increasing the bioavailability of these agents. Less favorable properties of these DDS include limited shelf life and administration route due to poor chemical and mechanical stability. In addition, designing these types of particles is more difficult (Barbé et al., 2004). Polymeric particles, partially overcome these limitations and can be categorized in natural and synthetic polymeric NPs. Potential antigenicity and poor batch-to-batch reproducibility are an impediment to the use of natural polymeric NPs (Reverchon et al., 2012; Andronescu and Grumezscu, 2017). On the other hand, synthetic polymers release acidic byproducts during degradation, raising a toxicity issue (Liechty et al., 2010). In comparison to other types of NPs, mesoporous silica nanoparticles (MSNPs) show large potential. Silica is already an additive in medical formulations. In addition, these particles offer biocompatibility and biodegradability, relatively high chemical and mechanical stability, a variety of surface functionalization due to abundant silanol groups and a simple synthesis procedure which can easily be upscaled to industrial applications (Seré et al., 2018).

In this work, proof of concept is provided for the use of biodegradable MSNPs as a carrier of (tumor)proteins as an alternative for DC immunotherapy. We report the relatively simple one pot synthesis of carboxylic functionalized MSNPs. In a first stage, the synthesis procedure is reassessed and optimized. The effect of the washing alcohol on the functional groups, the optimal amount of carboxylation and the optimal silica precursor were studied by complete characterization and biodegradation. From these studies, the optimal synthesis procedure was determined significantly lowering the cost of the vaccine production. The selected particles were then conjugated with proteins and used for *in vitro* stimulation of DCs. Besides being a good cost-effective alternative, another strong feature of this NP-based vaccine is the ability to load the particles with immunomodulatory agents to amplify the immune stimulating effects and increase the efficacy of the vaccine.

2. EXPERIMENTAL SECTION

2.1. MSNP Synthesis and Characterization

This work is a refinement of our previously reported MSNP synthesis procedure (Seré et al., 2018). Therefore, the influence of different silica precursors and dialysis alcohols was assessed, and NPs with different functional groups were produced as a

TABLE 1 | MSNPs examined in this work.

Sample	Functional groups	Precursor	Alcohol
MSNP-OH	None	TEOS	TBA
MSNP-NH_2	Amine	TEOS	TBA
MSNP-COOH-l	Carboxyl 0.075 mmol	TEOS	TBA
MSNP-COOH-m	Carboxyl 0.15 mmol	TEOS	TBA
MSNP-COOH-h	Carboxyl 0.30 mmol	TEOS	TBA
MSNP-OH*	None	TPOS	TBA
MSNP-COOH*	Carboxyl 0.15 mmol	TPOS	TBA
MSNP-COOH**	Carboxyl 0.15 mmol	TEOS	EtOH

*refers to the type of silica precursor used. Samples with * were produced using TPOS in stead of TEOS. **represents particles washed with ethanol in stead of tert-butyl alcohol.

reference for characterization. **Table 1** lists the examined particles in this work.

First, 0.5 g hexadecyltrimethylammonium bromide (CTAB, *acros organics*) and 0.4 g triethanolamine (TEA, *acros organics*) were dissolved in 60 mL ultrapure water. The solution was heated to 80°C and 2.75 mmol tetraethoxysilane (TEOS, *Sigma-Aldrich*) or tetrapropyl orthosilicate (TPOS, *Sigma-Aldrich*) was added while continuously stirring. Next, the mixture was stirred for 24 h to achieve a colloidal state. The NPs were either functionalized with amine or carboxylic surface functionalization, or they were washed without further surface modifications. The carboxylic surface functionalization was performed adding 0.13 mmol extra silica precursor (TEOS or TPOS) and 0.15 mmol carboxyethylsilanetriol (CES, *Gelest*) in case of standard (medium) carboxylation, denoted as MSNP-COOH or MSNP-COOH-m. In this work, the amount of CES was varied. Particles with a low amount of CES (0.075 mmol) or high amount (0.30 mmol) are denoted as MSNP-COOH-l and MSNP-COOH-h, respectively. CES provides the desired functionalization and additional silica precursor stabilizes the incorporation of carboxyl groups on the particle surface. The structural differences between CES and TEOS/TPOS causes faster hydrolysis and condensation of CES on the particle surface, resulting in an unstable surface chemistry. Therefore, CES was added 20 min after the silica precursor in order to have both substances condensate on the NP core simultaneously. Amine functionalized particles were produced by adding 0.13 mmol silica precursor and 0.13 mmol (3-aminopropyl) triethoxysilane (APTES, *Sigma-Aldrich*). For both functionalization types, the mixture was stirred for another 24 h at 80°C. After NP synthesis, the CTAB template was removed by dialysis (dialysis tubing membrane 14 kDa molecular weight cut off (MWCO), *Sigma-Aldrich*) of the NPs in 250 mL ultrapure water, 280 mL tert-butyl alcohol (TBA), or 280 mL ethanol (MSNP-COOH**) and 2.5 M aqueous acetic acid solution (*Sigma-Aldrich*) whilst vigorously stirring. Two different washing alcohols were tested to verify their influence on the carboxylic surface functionalization in acidic conditions. This mixture was refreshed five times after 12 h, afterwards replaced by ultrapure water and refreshed another five times until a neutral pH was reached.

The NP concentration was determined by centrifuging 1 mL MSNP solution for 10 min at 12,000 rcf to precipitate the particles. The sample was frozen and defrosted to destabilize the remaining particles in solution, and centrifuged again. Afterwards, the supernatant was removed and the precipitate was freeze dried under vacuum for 2 days (Alpha 1–4 LSC, *Martin Christ*). The dry particles were weighed to determine the concentration per milliliter.

Finally the MSNPs were fully characterized by a variety of techniques. The surface chemistry was determined with thermogravimetric analysis (TGA, STA 449 F1 *Netzsch*), Fourier transform infrared spectroscopy (FTIR, FTIR spectrometer Vertex 80v *Bruker*) and zeta potential (WALLIS zeta potential analyzer, *Cordouan Technologies*) measurements in function of the pH of the solution. Transmission electron microscopy (TEM, ARM200F *JEOL*) was performed at 200 keV after drying 10 μL of NP solution on a holey carbon-coated copper grid (*Agar Scientific*) under ambient conditions. The images were afterwards analyzed with ImageJ (Schneider et al., 2012), at least 100 NPs were taken into account to determine the core diameter.

2.2. Biodegradation of MSNPs and Spectrophotometric Determination of Silicate With Molybdenum Blue

The biodegradation procedure and analysis were based on our previous work (Seré et al., 2018). In order to verify the degradation of particles in the administration fluid for patients, the degradability was examined in saline solution in stead of PBS. The set-up remained similar, 6 mL of NPs was transferred to a dialysis membrane (dialysis tubing membrane 7 kDa MWCO, *Sigma-Aldrich*) and dialyzed against 100 mL 0.9% sodium chloride. In the first stage of degradation, a sample was taken every hour and the saline solution was refreshed to prevent concentration built-up of silicates [$Si(OH)_4$]. Gradually the time intervals prolonged as the degradation speed has been shown to decrease with increasing time (Seré et al., 2018).

The spectrophotometric determination of the amount of silicates and subsequent analysis was performed as described earlier (Seré et al., 2018).

2.3. Conjugation of MSNP With OVA and FITC

To prepare the nanovaccine, carboxylic functionalized MSNPs (MSNP-COOH) underwent standard carbodiimide cross linking chemistry using N-hydroxysulfosuccinimide (sulfo-NHS, *Thermo Fisher*) and N-(3-Dimethylaminopropyl)-N-ethylcarbodiimide hydrochloric acid (EDC, *Sigma-Aldrich*). For this, an activation mixture of 50 mM buffer 2-(N-morpholino)ethanesulfonic acid sodium salt (MES, *Sigma-Aldrich*), 50 mM sulfo-NHS and 25 mM EDC was prepared in ultrapure water. After adding the particles to the activation mixture at an end concentration of 1 mg/mL, they were left to react on a rotary wheel for 10–15 min. Next, 2 mg/mL OVA (*Sigma-Aldrich*) was added, and the mixture was left to react for 1 h while rotating. The conjugated particles (MSNP-COOH-OVA) were either immediately added to a DC culture, or ultrafiltrated (vivaspin 2 10000 MWCO PES VS0201, *VWR*) in case they were stored overnight to separate the

activation mixture from the nanovaccine. The vivaspin filtration membranes were washed 3 times before use with 2 mL ultrapure water and centrifugation at 1,000 g for 3 min. After filtration, the MSNP-COOH-OVA residue was recovered by resuspension in 1 mL ultrapure water and reverse spinning it into the recovery cap. Finally, the vaccine was administered to DCs at a concentration of 100 μg MSNPs and 200 μg OVA per million cells.

The NP uptake by DCs was investigated by labeling the MSNPs with 5-(aminoacetamido)fluorescein (fluoresceinyl glycine amide) (FITC, *Thermo Fisher*) using the same sulfo-NHS, EDC chemistry. FITC was added after activation of the carboxyl groups at a concentration of 0.25 mM and left on the rotary wheel for 1 h. Afterwards, the excess of FITC was separated from the labeled MSNPs (MSNP-COOH-FITC) using ultrafiltration as discussed in previous paragraph.

2.4. DC Generation and Culturing

The generation and maintenance of bone marrow derived DCs were based on the protocol of Belmans et al. (2017). First, DC culture medium was prepared using RPMI-1640 medium (*Thermo Fisher*), 10% FCS (*Thermo Fisher*), L-glutamine (*Thermo Fisher*), pen/strep (*Thermo Fisher*), 50 μM β-mercaptoethanol (*Sigma*), and 20 ng/mL granulocyte-macrophage colony-stimulating factor (GM-CSF, *Peprotech*). Bone marrow was collected from the femur and tibia of 8–10 weeks old female C57BL/6J mice (*envigo*). The bone marrow was flushed with PBS, the progenitor cells were counted (ABX Micros 60, *Horiba*) and finally cultured at one million cells per mL DC medium. The medium was refreshed on the third and fifth day of the culture. On the sixth and seventh day, the cells were prepared for confocal microscopy and flow cytometry, respectively.

2.5. Confocal Microscopy Staining

On the sixth day of the culture, immature DCs (iDCs) were collected, counted, and seeded onto coverslips. After 24 h of incubation, on day 7, DCs were treated with MSNP-COOH-FITC. Both iDCs (untreated) and mature DCs (mDCs) were used as control groups. The latter were treated with 1 μg/mL Escherichia coli lipopolysaccharide (LPS, *Sigma-Aldrich*). The cells were incubated for another 24 h before staining. They were then washed three times with PBS and incubated at 4°C for 10 min with fragment, crystallizable receptor blocker (FC-block, Anti-Mouse CD16/CD32 clone 93, *ebioscience*). Subsequently, the cells were further incubated at 4°C for 30 min while stained for MHC class I (H-2Kb-PE-Cy7 clone AF6-88.5.5.3, *ebioscience*). DCs underwent another washing procedure with PBS, were then fixed for 20 min at room temperature, followed by a final wash. Confocal microscopy images were analyzed using Fiji after recording on a Zeiss LSM 880—Airyscan (Cell and Tissue Imaging Cluster, KU Leuven) (Schindelin et al., 2012).

2.6. Flow Cytometry Staining

On the seventh day of the culture, DCs were treated with MSNPs, OVA, or MSNP-COOH-OVA. After 90 min incubation at 37°C, treated DCs were matured with LPS. iDCs and mDCs were used as control groups. After 24 h, the cells were collected and stained. The flow cytometry panel was based on the work of Baert et al. (2016) CD11c is typically highly expressed by DCs, an anti-CD11C mAb was therefore used to distinguish DCs from other cells in our samples. Fixable Viability Dye (FVD eFluor 506) was used to exclude dead cells from the data sets. This dye penetrates the compromised cell membranes of dead DCs and reacts with intracellular proteins. Costimulary molecules (CD40, CD86, CD80) and MHC class I and II molecules were stained as maturation markers. In addition, cells were stained for SIINFEKL/H-2Kb interaction. This mAb marked cross-presentation of the $OVA_{257-264}$ octapeptide SIINFEKL on MHC class I molecules. The used clones are listed in **Table 2**. Finally, flow cytometry was performed using a LSR Fortessa Analyzer (*BD Biosciences*) and analyzed with FlowJo software (*Tree Star*). The gating strategy is included in the **Supplementary Figure 2**.

TABLE 2 | Murine DC antibodies used in this work.

Antigen	Fluorochrome	Clone	Supplier
CD11c	Allophycocyanin	N418	eBioscience
CD80	PE-Cy7	16-10A1	eBiosciene
CD86	PE-Cy7	GL1	BD Bioscience
MHC-I (H-2Kb)	PE-Cy7	AF6-88.5.5.3	eBioscience
MHC-II (I-A/I-E)	PE-Cy7	M5/114.15.2	eBioscience
CD40	PE-Cy7	3/23	BioLegend
SIINFEKL/H-2Kb	PE	eBio25-D1.16	eBioscience

3. RESULTS AND DISCUSSION

3.1. MSNP Characterization and Optimization

A limited number of attempts have been made to produce carboxyl functionalized MSNPs in a one-pot process (Han et al., 2007; Kozlova and Kirik, 2010; Gu et al., 2013). Most groups report a complex post-synthesis process consisting of multiple steps (Yang et al., 2003; Chen et al., 2011; Han et al., 2011; Soo et al., 2019). To obtain a cost-effective alternative, we developed a simple one-pot wet chemistry process which is scalable to produce industrial quantities. The optimization of the protocol consisted of complete characterization, followed by improvements of experimental parameters, such as washing alcohol, functionalization precursor, and silica precursor.

3.1.1. Effect of the Washing Alcohol

In a first stage, the influence of the washing alcohol on carboxylic surface functionalization in acidic conditions was assessed. In previous work, ethanol was used to remove the structure directing agent (Yamada et al., 2012; Seré et al., 2018). Inefficient protein conjugation with these particles suggested Fischer esterification of the carboxyl groups when the template was removed with ethanol (Master Organic Chemistry LLC, 2020). To prevent this reaction, NPs were washed with TBA instead. TBA offers more steric hindrance, inhibiting the electrophilic carbon of the carboxylic acid to attack the alcohol. It is therefore less reactive than ethanol. Functionalization of these particles was first assessed with FTIR represented in **Figure 1**. Non-functionalized particles (MSNP-OH, blue curve)

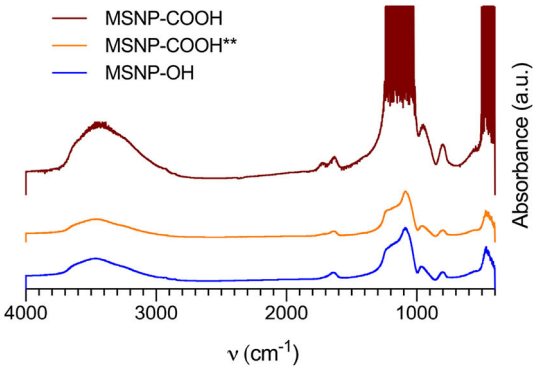

FIGURE 1 | FTIR spectra of non-functionalized MSNPs (MSNP-OH, blue), and carboxy-MSNPs washed with TBA (MSNP-COOH, red) or ethanol (MSNP-COOH**, orange). The characteristic absorption bands for carboxylic functionalization are visible in the TBA washed samples, to a lesser extend in the ethanol washed samples. Non functionalized particles did not show these characteristic bands.

show absorption bands at 480 cm^{-1} corresponding to O–Si–O bending, 800 cm^{-1} for Si-O bending, 950 cm^{-1} for SiO-H bending, in the range of 1,000–1,200 cm^{-1} for Si–O–Si stretching and a broad band around 3,500 cm^{-1} for SiO–H stretching. The band at 1,640 cm^{-1} is probably due to scissor bending vibrations of molecular water. Coating the particle surface with carboxyl groups, introduces additional bands at 1,720 cm^{-1} corresponding with the C=O stretch and 1,420 cm^{-1} which corresponds to the C–O stretch. The latter band is slightly visible in the FTIR spectrum of TBA washed particles (MSNP-COOH, red curve in **Figure 1**), but not present for ethanol washed particles (MSNP-COOH**, orange). Other infrared absorption bands characteristic for carboxyl groups, such as the O–H and C–H stretching band at 3,500 cm^{-1} and the O–H bending at 950 cm^{-1}, overlap with the spectrum for non-functionalized particles.

In essence, the FTIR spectra gave a first indication of successful carboxylic functionalization of MSNPs, especially for TBA washed MSNPs. The distinctive absorption bands for carboxyl groups are less abundant for ethanol washed particles, confirming the Fisher esterification hypothesis. It was therefore decided to use TBA during template removal.

SAXS and TEM analysis confirmed the mesoporous structure (**Supplementary Figure 1** and **Figure 5**). Zeta potential and TGA were performed for aforementioned samples and amine functionalized particles (MSNP-NH_2) in order to assess the grafted functional groups. **Figure 2A**, shows the zeta potential as a function of pH for MSNPs with different surface functionalization. The shape of the curve confirms successful carboxylic surface functionalization. As a reference, the isoelectric point (IEP) is considered. Non-functionalized MSNPs have an IEP at a pH value of 3.5. This value shifts to 6.7 for MSNP-NH_2, due to the change of surface charge. MSNP-COOH show no IEP as the zeta potential of these samples is negative over the complete pH range, confirming efficient carboxylic surface functionalization. Following the same reasoning, the shift of MSNP-COOH toward lower zeta potential values in the higher pH range suggests more carboxyl groups as compared to ethanol washed particles (MSNP-COOH**).

TGA decomposition profiles give a quantitative indication of the functional groups and were normalized to the weight of dry samples. This weight was set at 150°C, after removal of impurities and adsorbed moisture (Musso et al., 2015). Three regions can be observed for samples with functional groups and each can be ascribed to a certain surface chemistry (Gallas et al., 2009; Kozlova and Kirik, 2010; Musso et al., 2015). The first region from 150 to 370°C for carboxylated MSNPs and from 150 to 500°C for MSNP-NH_2, is attributed to the loss of silanol groups. The decomposition profile of carboxylated MSNPs shows a plateau before going into the second region ranging from 440 to 700°C. This steep decline is ascribed to the carboxylic surface functionalization. Amine functionalized MSNPs show a steep slope in the range from 500 to 700°C, representing amine functionalization. The gradual weight loss when increasing the temperature beyond 700°C is ascribed to further dehyroxylation. The TGA curves in **Figure 2B** demonstrate that the particles are grafted with carboxyl groups. The curves of carboxylated MSNP coincide for both washing methods in the first region, indicating an equal amount of silanol groups. In the second region, which represents the carboxylic surface functionalization, the TBA washed particles (MSNP-COOH) show slightly more weight-loss than ethanol washed particles (MSNP-COOH**). This confirms a higher amount of carboxyl groups, supporting the esterification hypothesis for ethanol washed particles.

The particles were degraded in 0.9% NaCl solution and molybdenum blue chemistry was used to assess the degradation kinetics shown in **Figure 3**. The results indicate that degradation occurs fastest for amine functionalized particles (green curve), followed by non-functionalized (blue curve) and carboxylated particles (orange and red curve). It has been shown that the negatively charged ions of a medium are the main mediators for particle degradation (Seré et al., 2018). The fast degradation for amine functionalized MSNPs can therefore be ascribed to the attractive electrostatic interactions between the degrading ions and the positively charged particles. Both silanol groups of non-functionalized particles as well as carboxyl groups of carboxy-MSNP, repel the negative ions. Due to the larger negative potential of carboxylated MSNPs, repulsion is higher and degradation therefore slower as compared to non-functionalized particles. As for the particles produced with different template removing alcohols, TBA washed particles (MSNP-COOH, red curve) degrade slower than ethanol washed particles (MSNP-COOH**, orange curve). Data in **Figure 2A** show that ethanol washed particles have lower absolute zeta potential values, suggesting a decreased ability to repel the degrading ions and resulting in faster degradation.

Based on these results, we conclude that the washing procedure has an impact on the surface functionalization. In addition, TBA washed particles degrade slightly slower, increasing their availability for DCs. We therefore selected TBA as the better washing alcohol for further NP production in this work.

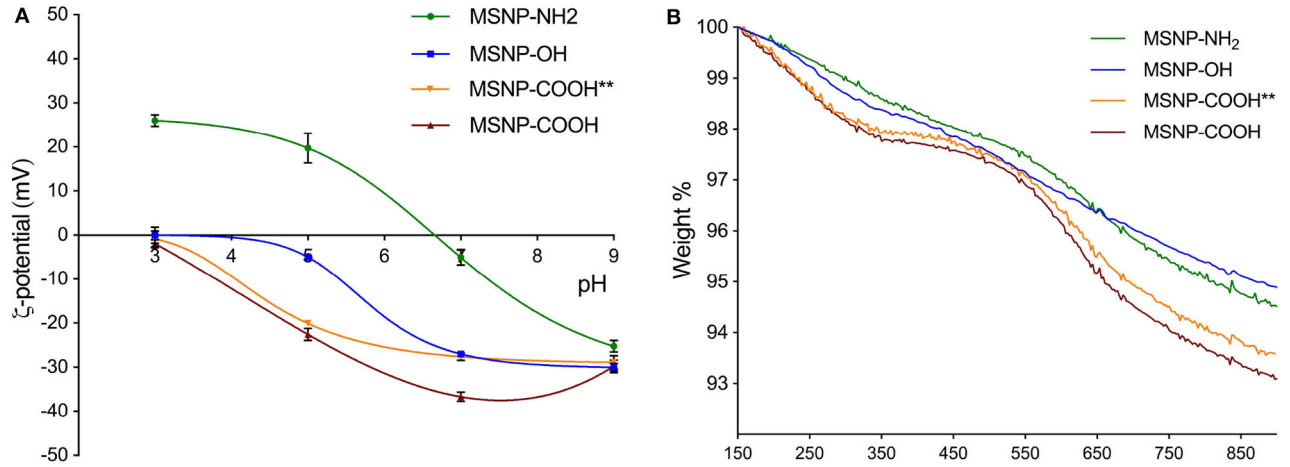

FIGURE 2 | (A) Zeta potential as a function of pH for MSNP-OH (blue), MSNP-NH_2 (green), MSNP-COOH (red), and MSNP-COOH** (orange). The first IEP occurs for MSNP-OH in the lower pH region, followed by MSNP-NH_2 in at high pH values. MSNP-COOH have a negative potential over the complete pH range and therefore do not show an IEP. The shift of the curve offers a first indication of the surface functionalization. **(B)** TGA decomposition profiles for MSNP-OH (blue), MSNP-NH_2 (green), MSNP-COOH (red), and MSNP-COOH**(orange). The first temperature window of the decomposition curves is attributed to the loss of silanol groups, followed by the range characteristic for the functional groups. These are 440–700 and 500–700°C for MSNP-COOH and MSNP-NH_2, respectively.

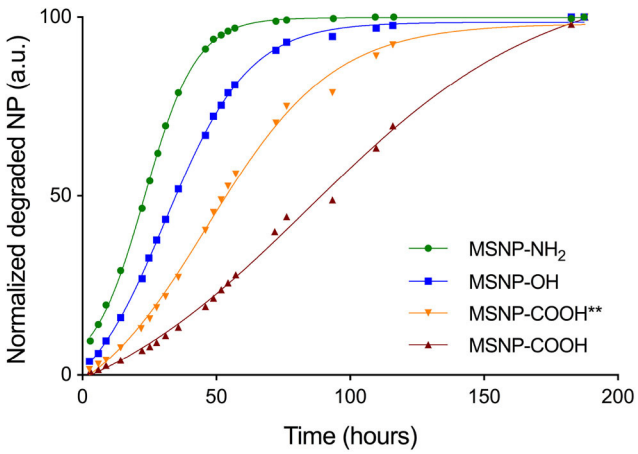

FIGURE 3 | Degradation kinetics for MSNP-OH (blue), MSNP-NH_2 (green), MSNP-COOH (red), and MSNP-COOH** (orange). Fast degradation of MSNP-NH_2 is due to the attractive electrostatic interaction of the particle with the degrading ions. MSNP-OH and carboxy-MSNP both repel the negatively charged ions of the solution. However, carboxy-MSNP have a larger negative potential and will therefore degrade slower. Finally, the zeta potential is more negative for TBA washed carboxy-MSNPs (MSNP-COOH), as compared to ethanol washed carboxy-MSNPs (MSNP-COOH**), causing slower degradation of MSNP-COOH.

3.1.2. Optimal Carboxylation

After improving the washing procedure, the optimal amount of CES for carboxylation was determined. Carboxylic surface functionalization of mesoporous silica materials using the CES precursor, has mainly received attention in the catalytic research field where SBA-15 sieves are functionalized (Han et al., 2007; Tsai et al., 2009). In addition, it is also used for carboxylic mesoporous silica coating of superparamagnetic iron oxide NPs (Sharifi et al., 2013). Other groups produced MSNP-COOH by producing 5-(Triethoxysilyl)pentanoic acid and incorporating it in a one-pot synthesis. The silica end of this carboxyl precursor resembles the TEOS structure more closely but requires another synthesis step (Feinle et al., 2017). Keeping the industrial scaling and costs in mind, water soluble CES was used in this work. Traditional co-condensation might cause the formation of additional silica entities in the solution, especially when higher amounts are used. Earlier research could therefore only implement trace amounts of CES (Gu et al., 2013; Sharifi et al., 2013). Since this work improved the functionalization route, the optimal carboxylation was investigated.

MSNP-COOH samples were produced following the standard protocol and using TBA to remove the CTAB template. The samples were denoted as MSNP-COOH-l, MSNP-COOH-m, and MSNP-COOH-h as the amount of CES was varied 0.075, 0.150, and 0.300 mmol, respectively. **Figure 4A** represents zeta potential measurements. Incorporating more carboxyl groups on the particle surface, increases inter-particle repulsion in the higher pH range (Duffy and Hill, 2011). It results in a higher zeta potential and more stable NPs. MSNP-COOH-h samples in **Figure 4A** (triangle full line) do not follow this expected trend. The progression of the zeta potential curve deviates, suggesting saturation of the NP surface when higher amounts of CES are used during synthesis.

The amount of grafted carboxyl groups was estimated with TGA. The normalized decomposition profiles are illustrated in **Figure 4B** and associated results in **Table 3**. The first temperature region from 150 to 370°C, represents the mass loss due to silanol groups. MSNP-COOH-l show more mass loss in this window as compared to the other two samples. The mass loss due to silanol groups of MSNP-COOH-m and MSNP-COOH-h samples is equal. This suggests an unsaturated particle surface

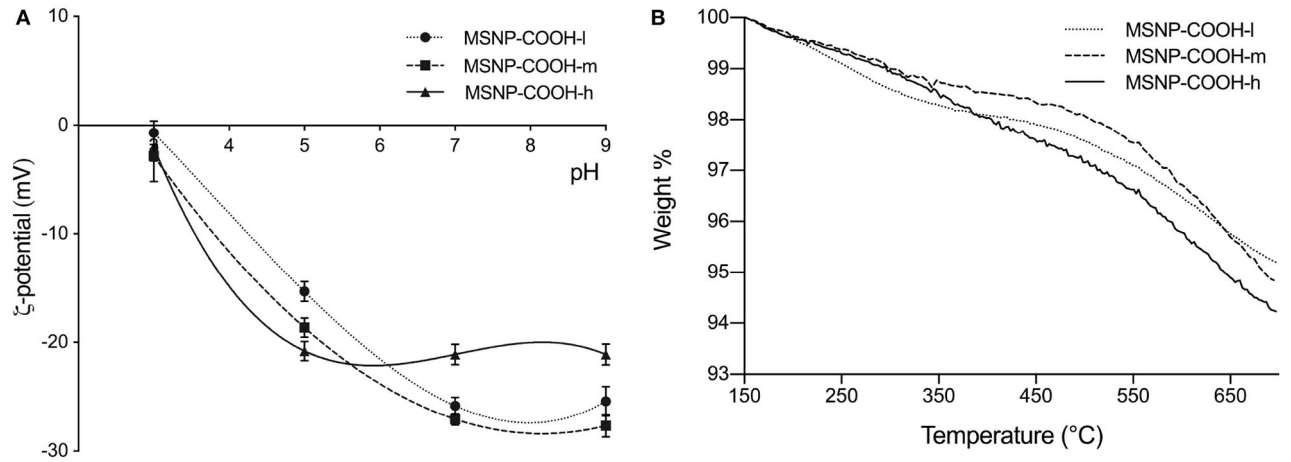

FIGURE 4 | (A) Zeta potential as a function of pH for MSNP-COOH-l, MSNP-COOH-m, and MSNP-COOH-h. NPs are expected to be more stable in the higher pH range, when more carboxyl groups are incorporated. MSNP-COOH-h do not follow this trend, suggesting surface saturation. **(B)** TGA decomposition profiles of MSNP-COOH-l, MSNP-COOH-m, and MSNP-COOH-h. MSNP-COOH-l show more mass loss in the silanol range, as compared to the other two samples. Mass loss in thisl region is equal for MSNP-COOH-m and MSNP-COOH-h. MSNP-COOH-m and MSNP-COOH-h show equal mass loss in the COOH characteristic window. Low amount of CES during synthesis renders particles with unsaturated surface. Saturation of the surface occurs (MSNP-COOH-m), and therefore no increase in functional groups occurs when even more CES is used (MSNP-COOH-h).

TABLE 3 | TGA decomposition of carboxy-MSNPS.

Sample	Weight loss silanol (150–370°C) (%)	Weight loss carboxyl (440–700°C) (%)
MSNP-COOH-l	1.4	2.6
MSNP-COOH-m	1.0	3.6
MSNP-COOH-h	1.0	3.6

when functionalized with 0.075 mmol CES; while adding 0.15 mmol CES or more, decreases the amount of silanol groups to a constant value, indicating particle saturation. The same trend is observed in the temperature range ascribed to the weight loss of carboxyl groups from 440 to 700°C. The amount of carboxyl groups is lower when a low amount of CES (0.075 mmol) is used. On the other hand, amount of grafted carboxyl groups is the same for both 0.15 and 0.30 mmol CES. An equal amount of carboxyl groups suggests saturation of the NP surface, which occurs due to steric hindrance of the carboxyl groups. Adding more CES results therefore in the same amount of carboxylic surface functionalization.

Particles functionalized with 0.15 mmol CES were considered to be optimal for protein loading, as this amount seems to saturate the particle surface.

3.1.3. Optimal Silica Precursor

Finally, in search of the optimal particle, two different silica precursors were examined. TEOS is a well-known and widely used precursor, a standard in the synthesis of silica NP synthesis (Rahman and Padavettan, 2012; Wu et al., 2013; Liberman et al., 2014; Zulfiqar et al., 2016). TPOS is known to render slightly larger particles and larger size distribution due to a lower hydrolysis rate during synthesis (Yamada et al., 2012). The size of TPOS based NPs would still be suitable for passive targeting of DCs (Yamada et al., 2012). Large particulate systems are mainly taken up by DCs, then transferred toward the lymph nodes where they stimulate the $CD8^+$ T-cells. By contrast, smaller particles are taken up by macrophages in the skin which are considered to be tissue resident (Manolova et al., 2008). We therefore aim to produce MSNPs between 20 and 50 nm in this work. In addition, the system's diameter increases with 300–500 nm by coating the MSNPs with tumor proteins to produce the nanovaccine. Therefore, NP monodispersity is not required, as the conjugation of peptides and proteins causes polydispersity of the final product. Our hypothesis is that slower hydrolysis during synthesis could result in more stable particles with regard to biodegradation, arousing interest in TPOS based particles.

TEOS or TPOS silica precursor (2.75 mmol) were used during synthesis and both non-functionalized and carboxy-MSNP were produced for further characterization. **Figures 5**, **6** show typical TEM images and the size distribution of carboxy-MSNP produced with TEOS (MSNP-COOH) and TPOS (MSNP-COOH*), respectively. As expected, TPOS based particles are larger with an average core diameter of (48 ± 8) nm. The TEOS precursor rendered smaller particles with an average diameter of (29 ± 4) nm. In addition, the size distribution of TPOS based particles is larger.

The MSNPs were characterized using zeta potential, TGA, and biodegradation experiments. Zeta potential and TGA data were comparable for TEOS and TPOS based nanoparticles, for both non-functionalized as well as carboxy-MSNP (data not shown). Thus, the silica precursor does not influence the electrochemical stability of the particles in solution, nor does it affect the surface chemistry. Biodegradation experiments were performed in 0.9% sodium chloride and results are shown

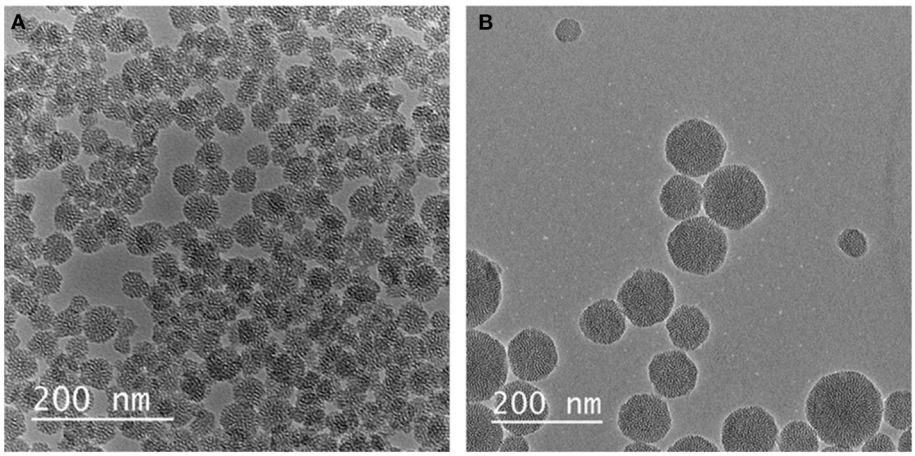

FIGURE 5 | Representative TEM images of **(A)** MSNP-COOH and **(B)** MSNP-COOH*.

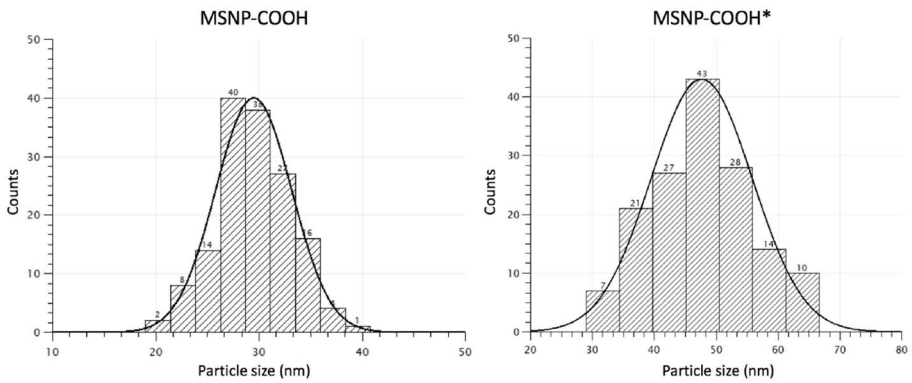

FIGURE 6 | Size distribution MSNP-COOH (TBA washed) and MSNP-COOH* (ethanol washed) based on TEM measurements. The size distribution is narrower when CTAB templates are washed with TBA during synthesis.

in **Figure 7**. All MSNPs degraded in saline solution. The degradation behavior of non-functionalized and carboxylated MSNPs is in line with aforementioned conclusions. Particles with carboxylic surface chemistry degrade slower due to the repulsive interaction with the degrading ions in the medium. In contrast to our expectations, TEOS based particles degrade slower than particles synthesized with TPOS comparing particles with identical functionalization. The degradation curves follow the same course, but are shifted when TEOS is used for core synthesis. At a degradation of 50%, the curve is shifted for 12 and 18 h in case of non-functionalized and carboxylated MSNPs, respectively. The effect of the silica precursor is in contrast to what is expected from the study of Yamada et al. (2012). Probably, the synthesis route used in this work, affects the pore and particle size and hence the biodegradability. Slower degradation implies more chance of DCs to take up the nanovaccine in the human body.

The optimal particles for this work were MSNP-COOH, synthesized with a TEOS precursor, functionalized with 0.15 mmol CES and washed with TBA.

3.2. *In vitro* Assessment of MSNPs and the Nanovaccine

3.2.1. Dose-Response Relationship Between MSNPs and DCs

The first *in vitro* steps were taken by determining the optimal MSNP dose to treat and analyze DCs. The dose response relationship between MSNPs and the viability of DCs is shown in **Figure 8A**. The graph was established by culturing DCs and exposing them to MSNPs. After flow cytometry acquisition, the viability was determined using an adjustment of the general gating strategy in **Supplementary Figure 2**. Single cell selection (**Supplementary Figures 1A,B**) was followed by extracting the $CD11c^{+}$, FVD^{-} populations in a single gate as represented in **Figure 8B**. Control conditions were taken into account with iDCs (untreated) and mDCs (LPS stimulated). The test conditions consisted of DCs incubated with: 50, 100, 200, and 400 μg MSNPs per million DCs. Each NP treated DC culture received an LPS stimulation signal 90 min after the particles were introduced. Data were pooled from two experiments containing five cultures per condition.

The main factors affecting NP cytotoxicity are surface functionalization, size, and concentration. Although MSNPs are known to be biocompatible and biodegradable, their cytotoxicity significantly increased when their concentration increased as shown in **Figure 8**. Anova pairwise comparison was used to determine statistical significance, using iDC and mDC as control conditions. No significant difference was observed when DCs were treated with 50 or 100 μg MSNPs per million DCs. Increasing the quantity of MSNPs significantly decreased DC viability (***$p \leq 0.001$). The threshold toward cytotoxicity for the NPs in this work was set at 100 μg per million DCs and was therefore used as standard for loading DCs. In addition, the viability of DCs treated with 50 or 100 μg MSNPs was significantly higher than DCs treated with higher NP doses (not indicated on graph).

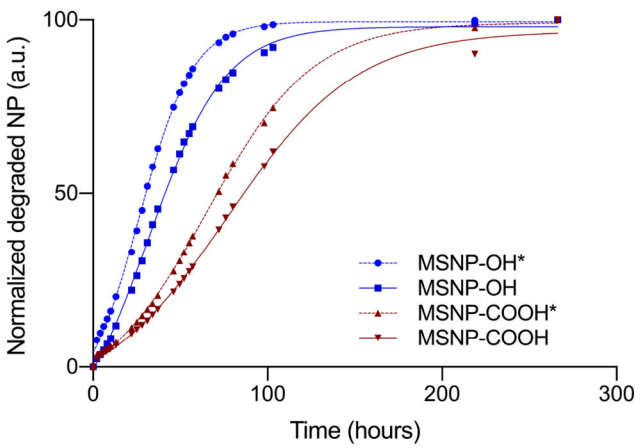

FIGURE 7 | Degradation behavior of non-functionalized and carboxy-MSNP, produced with TEOS and TPOS (*). The shape of the degradation curve is the same for particles with identical functionalization, regardless the silica precursor used during synthesis. Curves shifts to the right for TEOS based particles, indicating slower degradation.

3.2.2. MSNP and Nanovaccine Uptake by DCs

The uptake of particles and nanovaccine by DCs was examined using confocal microscopy. First, DCs were incubated with labeled MSNPs (MSNP-FITC), stimulated with LPS and stained for MHC class I molecules. To gain a better insight in the uptake process, half of the cells were incubated at 4°C and the other half at normal physiological temperatures, i.e., 37°C. The results are illustrated in **Figure 9**. **Figures 9A,B** show images of MSNP treated DCs, incubated at 37°C. The green signal was attributed to the FITC labeled MSNPs, the red signal to PE-Cy7 labeled MHC class I molecules. Since MHC class I molecules are membrane molecules, they visualize the cells' exterior. The green signal of MSNPs is concentrated inside the red MHC signal. No particles were observed being attached to the cell surface, indicating cellular uptake of the MSNPs. In addition, **Figures 9C,D**, display the uptake mechanism since these cells were incubated at different temperatures. It is known that cell metabolism shuts down at 4°C (**Figure 9C**) (De Vleeschouwer et al., 2005; Belmans et al., 2017). The absence of the green MSNP signal, stipulated no particle uptake by DCs. Incubation at 37°C on the other hand, did show particle uptake within the same experiment (**Figure 9D**). In conclusion this demonstrated that particle internalization is an active process (ATP dependent) and not merely NPs penetrating the membrane of DCs. This was an indication of endocytosis, meaning that particles and transported proteins enter the cross-presentation pathway.

Nanovaccine uptake, or at least the internalization of the transported tumor proteins, is of great importance to induce an anti-tumor immune response. To determine protein uptake

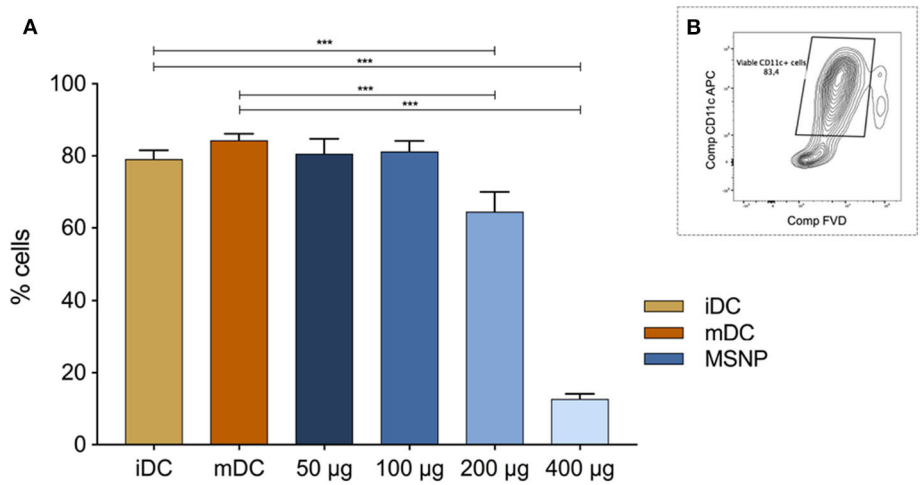

FIGURE 8 | (A) Shows the effect of various doses of MSNPs on the DC viability. iDC and mDC are the control conditions. Blue represents the viability of MSNP treated DCs. The doses included (from dark to light blue) 50, 100, 200, and 400 μg NPs per million DCs. **(B)** Pictures the gating strategy to select viable (FVD^-) DCs ($CD11c^+$). Anova multiple comparison was used to determine significance. The viability of DCs decreased significantly when incubated with 200 or 400 μg MSNPs per million DCs. *$p \leq 0.1$, **$p \leq 0.01$, and ***$p \leq 0.001$ are refers to statistical significance of the data.

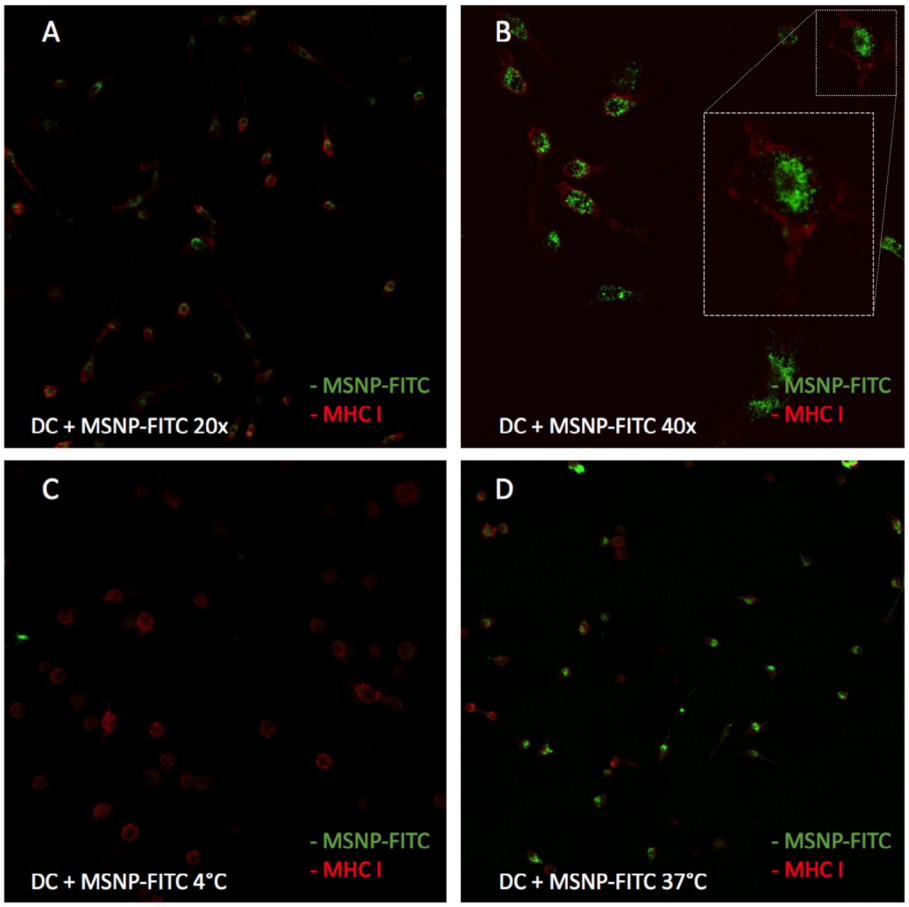

FIGURE 9 | Uptake of MSNPs by DCs. The red signal represents MHC class I molecules at the cell surface. The green signal represents the FITC label on the MSNPs. **(A,B)** Demonstrate NP uptake by DCs as the red signal of the cells' exterior encircles the green signal of the MSNPs. **(C,D)** Show the uptake of NPs when cells are incubated at 37 and 4°C, respectively. When cells are incubated at 4°C, the cell metabolism in shut down. A lack of green signal in **(C)**, represents no particle uptake. Therefore, the uptake is a determined to be an active process.

by DCs after treatment with the nanovaccine, MSNPs were loaded with OVA, Alexa Fluor 488 conjugates (OVA-Alexa). The same incubation and staining process was followed as for particle uptake. Confocal microscopy images confirmed uptake of OVA-Alexa, as shown in **Figure 10**. The green OVA signal is observed within the red MHC signal. Moreover, a yellow overlay of the green OVA signal and the red MHC class I signal was observed for several cells. This was a first suggestion of cross-presentation of OVA by DCs. The cross-presentation was quantitatively determined with flow cytometry.

3.2.3. Nanovaccine Effect on DCs and Cross-Presentation

In a first stage of these experiments, the effect of MSNPs on DCs was investigated by incubating the cells with as-synthesized and UV-sterilized particles. The effect of the nanovaccine was tested as well by incubating the cells with MSNP-OVA. The viability and maturation effect on the DCs were examined with flow cytometry. No significant difference was observed between the viability of treated DCs and control conditions iDC and mDC (data not shown). In addition, the sterilized particles were characterized and no changes were observed before or after sterilization. These results imply that the sterilization step can be included for further application as it does not negatively affect DCs, nor does it affect the quality of the NPs.

After demonstrating particle and vaccine uptake, the maturation effect of the treatment on DCs was examined. **Figure 11** shows the expression levels of the most important maturation markers of these cells, which include CD86, IA/IE, and CD40. MHC class I and CD80 expression levels were excluded from the data as these levels were high and comparable for all samples. The complete data can be found in the **Supplementary Figure 3**. The results were obtained by pooling data of six experiments with three cultures per condition per experiment.

iDCs showed low expression levels for the maturation markers, as expected (**Figure 11**, yellow). The immature state is typically specialized in sampling its environment *in vivo*. Increased expression of costimulatory molecules and MHC only takes place once pathogens are encountered and stimulation occurs. mDCs thus represented the positive control group for

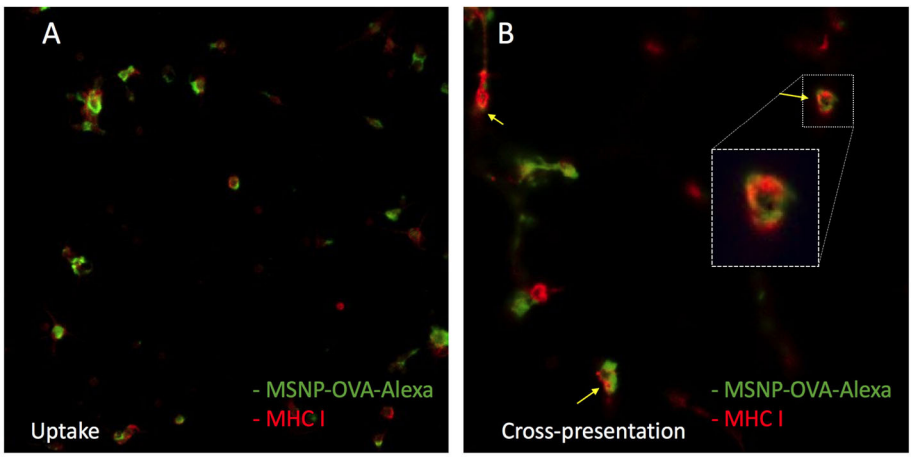

FIGURE 10 | Uptake of the model nanovaccine by DCs. The red signal represents MHC class I molecules at the cell surface. The green signal represents the alexa 488 labeled OVA. **(A)** Confirms nanovaccine uptake. **(B)** Shows a yellow overlay of the green and red signal, indicating cross presentation of OVA on MHC class I molecules.

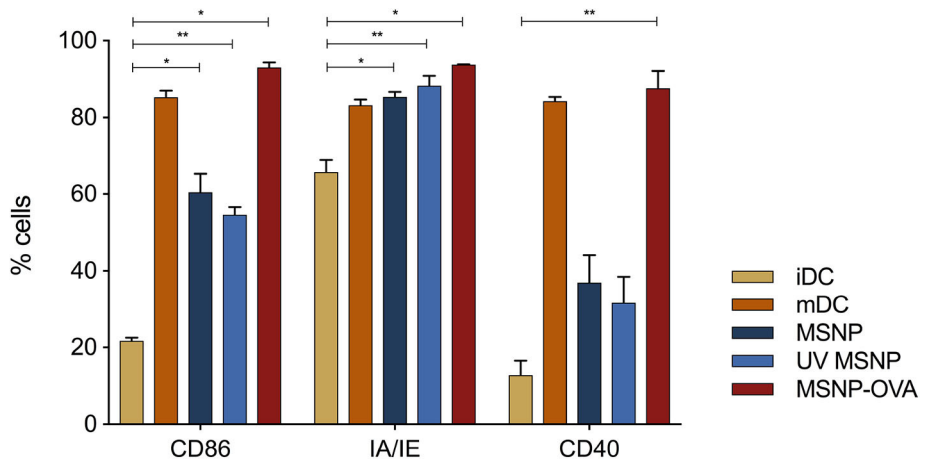

FIGURE 11 | Mean maturation expression levels of DCs are shown. iDCs and mDCs are control conditions, represented in yellow and orange, respectively. The expression levels of costimulatory and MHC molecules are clearly higher for mDCs. DCs treated with MSNPs (as-synthesized and UV sterilized), are represented in blue. No significant difference between DCs treated with sterilized and non-sterilized particles was observed. MSNP treated DCs show elevated expression levels of costimulatory and MHC molecules as compared to iDCs. Albeit the expression was not as high as mature DCs, indicating rather moderate maturation effect of MSNPs. The expression levels of DCs treated with the nanovaccine and stimulated with LPS are shown in red and are significantly higher than MSNP treated DCs and iDCs. $^{*}p \leq 0.1$ and $^{**}p \leq 0.01$ are refers to statistical significance of the data.

the maturation effect (**Figure 11**, orange). The expression levels of the shown markers was significantly higher for mDCs (Anova Dunnett's multiple comparisons test ($^{**}p \leq 0.01$), not indicated on the graph). DCs treated with particles alone (**Figure 11**, blue) did not receive a maturation trigger, in order to assess the effect of MSNPs. These DCs showed significantly increased expression levels of CD86 and MHC class II as compared to iDCs ($^{*}p \leq 0.1$ for MSNP and $^{**}p \leq 0.01$ for UV MSNP). In addition, higher expression of CD40 was observed. However, the expression levels of maturation markers were still lower than those of mDCs. These results were significant for CD40 ($^{*}p \leq 0.1$) and CD86 ($^{*}p \leq 0.1$ for MSNP and $^{***}p \leq 0.001$ for UV MSNP). We concluded that MSNPs have a moderate adjuvant effect on DCs and thus possibly the adaptive immune system. Incorporating immunomodulatory agents, such as TLR ligands (R848), on the particle surface could increase the stimulating effect further. In addition, DCs treated with MSNPs and UV sterilized MSNPs exhibited comparable expression levels of costimulatory and MHC molecules. As expected, DCs treated with the nanovaccine exhibited similar expression levels of MHC and costimulatory molecules as compared to mDCs (**Figure 11**, red, no significant difference). Both conditions were stimulated with LPS. The expression levels of DCs treated with the nanovaccine seemed even higher, which was possibly associated with the accumulative effect of LPS and NPs. MSNPs caused moderate maturation, which is further increased by LPS. These results indicated the adjuvant effect of MSNPs on DCs. which was a first suggestion of DCs being able to communicate the protein information delivered by NPs to the T-cells of the immune system.

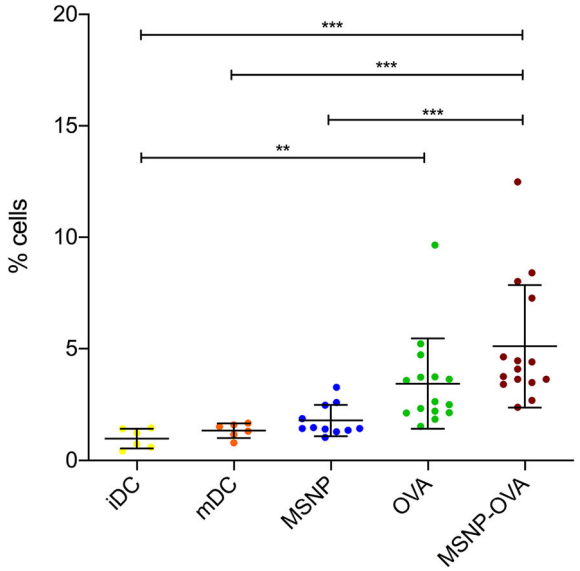

FIGURE 12 | Cross-presentation of the SIINFEKL peptide on MHC class I. iDCs and mDCs are control conditions, represented in yellow and orange, respectively. DCs treated with MSNPs, OVA and the model nanovaccine (MSNP-OVA) are represented in blue, green, and red, respectively. DCs treated with nanovaccine cross-presented the OVA antigen in higher levels. $^{*}p \leq 0.1$, $^{**}p \leq 0.01$, and $^{***}p \leq 0.001$ are refers to statistical significance of the data.

In order to investigate the cross-presentation of OVA on MHC class I molecules, DCs were loaded with the nanovaccine and cells were stained for flow cytometry with SIINFEKL-PE. This antibody stains the combination of the SIINFEKL peptide and MHC class I, and is therefore a quantitative indication of the cross-presentation of MSNP delivered OVA. The data and statistical analysis can be found in the **Supplementary Figures 4, 5** and **Supplementary Tables 1, 2**, results are shown in **Figure 12**. Data of four experiments were pooled, each experiment consisted of three to five groups per condition. Tukey HSD all pairwise comparison implicated significant differences between the cross-presentation of all negative control groups (i.e., iDC, mDC, and MSNP treated DCs) and DCs treated with the model nanovaccine ($^{***}p \leq 0.001$). In addition, cross-presentation of OVA on MHC class I by iDCs was significantly lower than OVA treated DCs ($^{**}p \leq 0.01$). A clear tendency toward higher cross-presentation was perceived when cells were treated with the nanovaccine. This indicated that DCs should be able to stimulate the CTLs of the immune system to specifically attack the tumor.

4. CONCLUSION

The MSNP synthesis and functionalization reported in this work consist of a one pot wet chemistry process which can easily be up-scaled to industrial production. The synthesis and functionalization, were optimized by assessing different silica precursors and different amounts of surface functionalization. These small manipulations during synthesis enable modification of physicochemical properties of the particles. MSNPs were produced within the desired size range (20–50 nm) for passive targeting of DCs after producing the nanovaccine. Characterization confirmed carboxylic surface functionalization necessary for subsequent protein conjugation. The developed MSNPs are resistant against agglomeration at experimental and physiological pH. In addition, they have shown to be biodegradable over a time span of 1 week, which is sufficiently long for DCs to take up the nanovaccine. This period was adjustable by varying the functionalization and silica precursor during synthesis. TEOS based MSNPs were found to be smaller but more resistant against biodegradation in comparison to TPOS based particles. Therefore, TEOS was preferred in further experiments. The optimal amount of carboxylic surface functionalization was reached using 0.15 mmol CES during NP synthesis.

NPs and the nanovaccine were taken up by DCs and this was found to be an active physiological process. Overlay of the MHC-I and OVA signal suggested the ability of DCs to cross-present proteins delivered by MSNPs. UV sterilization of the MSNPs did not induce any decrease in particle quality, nor did it have toxic effects on DC cultures. Treatment with MSNPs increased expression levels of MHC and costimulatory molecules of DCs in culture, indicating an adjuvant effect of the particles on DCs and possibly the adaptive immune system. Finally, cross-presentation was examined quantitatively with flow cytometry. Compared to control conditions, increased cross-presentation of OVA was observed when DCs were treated with the nanovaccine. These preliminary results confirm the large potential of MSNP based nanovaccines as a replacement of the expensive DC-based vaccines for active specific immunotherapy, offering a more standardized production process and possibly higher efficacy.

DATA AVAILABILITY STATEMENT

The raw data supporting the conclusions of this article will be made available by the authors, without undue reservation.

ETHICS STATEMENT

The animal study was reviewed and approved by Animal Ethics Committee KU Leuven.

AUTHOR CONTRIBUTIONS

The work in this article was part of the research activities of SS, in the framework of her doctoral dissertation. UV and SS collaborated and contributed equally. The research was performed in the group of J-PL and JS. SV and IL closely mentored the study and provided important input throughout the different phases of this work. All authors contributed to the article and approved the submitted version.

FUNDING

SS extends her gratitude to the Research Foundation-Flanders (Grant No. 1S52016N) for the Ph.D. scholarship.

JS acknowledges the Hercules Stichting (Project AKUL/13/19), funding the TEM. Finally, we want to acknowledge the Olivia Fund for their financial support.

ACKNOWLEDGMENTS

SS would like to extensively thank the research group of An Coosemans for making their lab and tools available, and for the excellent cooperation. Finally, we thank Carmen Bartic and Olivier Deschaume for the use of the spectrophotometer.

SUPPLEMENTARY MATERIAL

The Supplementary Material for this article can be found online at: https://www.frontiersin.org/articles/10.3389/fnano.2020.584233/full#supplementary-material

REFERENCES

Andronescu, E., and Grumezscu, A. M. (Eds.). (2017). *Nanostructures for Oral Medicine*. Elsevier.

Baert, T., Garg, A. D., Vindevogel, E., Van Hoylandt, A., Verbist, G., Agonistinis, P., et al. (2016). *In vitro* generation of murine dendritic cells for cancer immunotherapy: an optimized protocol. *Anticancer Res.* 36, 5793–5802. doi: 10.21873/anticanres.11163

Barbé, C., Bartlett, J., Kong, L., Finnie, K., Lin, H. Q., Larkin, M., et al. (2004). Silica particles: a novel drug-delivery system. *J. Adv. Mater.* 16, 1959–1966. doi: 10.1002/adma.200400771

Belmans, J., Van Woensel, M., Creyns, B., Dejaegher, J., Bullens, D., and Van Gool, S. (2017). Immunotherapy with subcutaneous immunogenic autologous tumor lysate increases muring glioblastoma survival. *Sci. Rep.* 7:13902. doi: 10.1038/s41598-017-12584-0

Chen, C., Pu, F., Huang, Z., Liu, Z., Ren, J., and Qu, X. (2011). Stimuli-responsive controlled-release system using quadruplex DNA-capped silica nanocontainers. *Nucleic Acids Res.* 39, 1638–1644. doi: 10.1093/nar/gkq893

De Jong, W. H., and Brom, P. J. A. (2008). Drug delivery and nanoparticles: applications and hazards. *Int. J. Nanomed.* 3, 133–149. doi: 10.2147/IJN.S596

De Vleeschouwer, S., Arredouani, M., Adé, M., Cadot, P., Vermassen, E., Ceuppens, J. L., et al. (2005). Uptake and presentation of malignant glioma tumor cell lysates by monocyte-derived dendritic cells. *Cancer Immunol. Immunother.* 54, 372–382. doi: 10.1007/s00262-004-0615-8

Dejaegher, J., Van Gool, S., and De Vleeschouwer, S. (2014). Dendritic cell vaccination for glioblastoma multiforme: review with focus on predictive factors for treatment response. *J. Immunotargets Ther.* 3, 55–66. doi: 10.2147/ITT.S40121

Delves, P. J. (Ed.). (1998). *Encyclopedia of Immunology, 2nd Edn.* Elsevier.

Duffy, J., and Hill, A. (2011). *Suspension Stability: Why Particle Size, Zeta Potential and Rheology Are Important*. Malvern: Malvern Instruments Ltd.

Feinle, A., Leichtfried, F., Straber, S., and Husing, N. (2017). Carboxylic acid-functionalized porous silica particles by a co-condensation approach. *J. Sol-Gel Sci. Technol.* 81, 138–146. doi: 10.1007/s10971-016-4090-4

Gallas, J. P., Goupil, J. M., Vimont, A., Lavalley, J. C., Gil, B., Gilson, J. P., et al. (2009). Quantification of water and silanol species on various silicas by coupling IR spectroscopy and *in-situ* thermogravimetry. *Langmuir* 25, 5825–5834. doi: 10.1021/la802688w

Galluzzi, L., Vacchelli, E., Bravo-San Pedro, J.-M., Buque, A., Senovilla, L., Baracco, E. E., et al. (2014). Classification of current anticancer immunotherapies. *Oncotarget* 5, 12472–12508. doi: 10.18632/oncotarget.2998

Gu, J., Liu, J., Li, Y., Zhao, W., and Shi, J. (2013). One-pot synthesis of mesoporous silica nanocarriers with tunable particle sizes and pendent carboxylic groups for cisplatin delivery. *Langmuir* 29, 403–410. doi: 10.1021/la3036264

Han, L., Sakamoto, Y., Terasaki, O., Lia, Y., and Che, S. (2007). Synthesis of carboxylic group functionalized mesoporous silicas (CFMSS) with various structures. *J. Mater. Chem.* 12, 1216–1221. doi: 10.1039/b615209k

Han, L., Terasaki, O., and Shunai Che, S. (2011). Carboxylic group functionalized ordered mesoporous silicas. *J. Mater. Chem.* 30, 11033–11039. doi: 10.1039/c1jm10561b

IARC (2018). *Latest Global Cancer Data: Cancer Burden Rises to 18.1 Million New Cases and 9.6 Million Cancer Deaths in 2018*. Press release N° 263. IARC.

Kozlova, S. A., and Kirik, S. D. (2010). Post-synthetic activation of silanol covering in the mesostructured silicate materials MCM-41 and SBA-15. *Microporous Mesoporous Mater.* 133, 124–133. doi: 10.1016/j.micromeso.2010.04.024

Le Gall, C. M., Weiden, J., Eggermont, L. J., and Figdor, C. G. (2018). Dendritic cells in cancer immunotherapy. *Nat. Mater.* 17, 472–477. doi: 10.1038/s41563-018-0093-6

Liberman, A., Mendez, N., Trogler, W. C., and Kummel, A. C. (2014). Synthesis and surface functionalization of silica nanoparticles for nanomedicine. *Surf. Sci. Rep.* 69, 132–158. doi: 10.1016/j.surfrep.2014.07.001

Liechty, W. B., Kryscio, D. R., Slaughter, B. V., and Peppas, N. A. (2010). Polymers for durg delivery systems. *Annu. Rev. Chem. Biomol. Eng.* 1, 149–173. doi: 10.1146/annurev-chembioeng-073009-100847

Makkouk, A., and Weiner, G. J. (2015). Cancer immunotherapy and breaking immune tolerance: new approaches to an old challenge. *Cancer Res.* 75, 5–10. doi: 10.1158/0008-5472.CAN-14-2538

Manolova, V., Flace, A., Bauer, M., Schwarz, K., Saudan, P., and Bachmann, M. F. (2008). Nanoparticles target distinct dendritic cell populations according to their size. *Eur. J. Immunol.* 38, 1404–1413. doi: 10.1002/eji.200737984

Marasini, N., Ghaffar, K. A., Skwarczynski, M., and Toth, I. (2017). *Micro and Nanotechnology in Vaccine Development*. Elsevier.

Master Organic Chemistry LLC (2020). *Conversion of Carboxylic Acids to Esters Using Acid and Alcohols (Fischer Esterification)*. Master Organic Chemistry LLC.

Mitra, A. K., Cholkar, K., and Mandal, A. (Eds.). (2017). *Emerging Nanotechnologies for Diagnostics, Drug Delivery and Medical Devices*. Elsevier.

Musso, G. E., Bottinelli, E., Celi, L., Magnacca, G., and Berlier, G. (2015). Influence of surface functionalization on the hydrophilic character of mesoporous silica nanoparticles. *Phys. Chem. Chem. Phys.* 17, 13882–13894. doi: 10.1039/C5CP00552C

Rahman, I. A., and Padavettan, V. (2012). Synthesis of silica nanoparticles by sol-gel: size-dependent properties, surface modification, and applications in silica-polymer nanocomposites–a review. *J. Nanomater.* 2012:132424. doi: 10.1155/2012/132424

Reverchon, E., Baldino, L., Cardea, S., and De Marco, I. (2012). Biodegradable synthetic scaffolds for tendon regeneration. *Muscl. Ligaments Tendons J.* 2, 181–186.

Riley, R. S., June, C. H., Langer, R., and Mitchell, M. J. (2019). Delivery technologies for cancer immunotherapy. *Nat. Rev. Drug Discov.* 18, 175–196. doi: 10.1038/s41573-018-0006-z

Schindelin, J., Arganda-Carreras, I., and Frise, E. (2012). Fiji: an open-source platform for biological-image analysis. *Nat. Methods* 9, 676–682. doi: 10.1038/nmeth.2019

Schneider, C. A., Rasband, W. S., and Eliceiri, K. W. (2012). NIH image to imagej: 25 years of image analysis. *Nat. Methods* 9, 671–675. doi: 10.1038/nmeth.2089

Seré, S., De Roo, B., Vervaele, M., Van Gool, S., Jacobs, S., Seo, J. W., et al. (2018). Altering the biodegradation of mesoporous silica nanoparticles by means of experimental parameters and surface functionalization. *J. Nanomater.* 2018:7390618. doi: 10.1155/2018/7390618

Sharifi, S., Daghighi, S., Motazacker, B., Sanjabi, B., Akbarkhanzadeh, A., Rowshani, S., et al. (2013). Superparamagnetic iron oxide nanoparticles alter expression of obesity and T2D-associated risk genes in human adipocytes. *Sci. Rep.* 3:2173. doi: 10.1038/srep02173

Soo, S., Jung, M. H., Lee, Y.-S., Bae, J.-H., Kim, S.-H., and Ha, C.-S. (2019). Functionalised mesoporous silica nanoparticles with excellent cytotoxicity against various cancer cells for pH-responsive and controlled drug delivery. *Mater. Des.* 184:108187. doi: 10.1016/j.matdes.2019.108187

Tsai, C. T., Pan, Y. C., Ting, C. C., Vetrivel, S., Chiang, A. S. T., Fey, G. T., et al. (2009). A simple one-pot route to mesoporous silicas SBA-15 functionalized

with exceptionally high loadings of pendant carboxylicic acid groups. *Chem. Commun.* 33, 5018–5020. doi: 10.1039/b909680a

Van de Velde, A. L., Anguilie, S., Beutels, P., Dom, S., Cornille, I., Nijs, G., et al. (2014). Cost analysis of immunotherapy using dendritic cells for acurate myeloid leukemia patients. *Blood* 124:1322. doi: 10.1182/blood.V124.21.1322.1322

Van Gool, S. (2015). Brain tumor immunotherapy: what have we learned so far? *Front. Oncol.* 5:98. doi: 10.3389/fonc.2015.00098

Van Gool, S., and De Vleeschouwer, S. (2012). Shoud dendritic cell-based tumor vaccination be incorporated into standard therapy for newly diagnosed glioblastoma patients? *Expert Rev. Neurother.* 12, 1–3. doi: 10.1586/ern.12.107

Wu, S.-H., Mou, C. Y., and Lin, H.-P. (2013). Synthesis of mesoporous silica nanoparticles. *Chem. Soc. Rev.* 42, 3862–3875. doi: 10.1039/c3cs 35405a

Yamada, H., Urata, C., Aoyama, Y., Osada, S., Yamauchi, Y., and Kuroda, K. (2012). Preparation of colloidal mesoporous silica nanoparticles with different diameters and their unique degradation behavior in static aqueous systems. *Chem. Mater.* 24, 1462–1471. doi: 10.1021/cm3001688

Yang, C., Zibrowius, B., and Schüth, F. (2003). A novel synthetic route for negatively charged ordered mesoporous silica SBA-15. *Chem. Commun.* 14, 1772–1773. doi: 10.1039/B304626E

Zulfiqar, U., Subhani, T., and Husain, S. W. (2016). Synthesis and characterization of silica nanoparticles from clay. *J. Asian Ceram. Soc.* 4, 91–96. doi: 10.1016/j.jascer.2015.12.001

Conflict of Interest: The authors declare that the research was conducted in the absence of any commercial or financial relationships that could be construed as a potential conflict of interest.